Applied Mathematics and Computation 320 (2018) 61–74

Contents lists available at ScienceDirect

Applied Mathematics and Computation

journal homepage: www.elsevier.com/locate/amc

# On the application of the method of fundamental solutions to boundary value problems with jump discontinuities

Carlos J.S. Alves[a,b,*], Svilen S. Valtchev[a,c]

[a] CEMAT–IST, University of Lisbon, Av. Rovisco Pais 1, 1049-001 Lisbon, Portugal
[b] Department of Mathematics, IST, University of Lisbon, 1049-001 Lisbon, Portugal
[c] Department of Mathematics, ESTG, Polytechnic Institute of Leiria, 2411-901 Leiria, Portugal

ARTICLE INFO

*Keywords:*
Harmonic boundary value problems
Singular boundary conditions
Meshfree method
Method of fundamental solutions
Enrichment technique

ABSTRACT

Two meshfree methods are proposed for the numerical solution of boundary value problems (BVPs) for the Laplace equation, coupled with boundary conditions with jump discontinuities. In the first case, the BVP is solved in two steps, using a subtraction of singularity approach. Here, the singular subproblem is solved analytically while the classical method of fundamental solutions (MFS) is applied for the solution of the regular subproblem. In the second case, the total BVP is solved using a variant of the MFS where its approximation basis is enriched with a set of harmonic functions with singular traces on the boundary of the domain. The same singularity-capturing functions, motivated by the boundary element method (BEM), are used for the singular part of the solution in the first method and for augmenting the MFS basis in the second method. Comparative numerical results are presented for 2D problems with discontinuous Dirichlet boundary conditions. In particular, the inappropriate oscillatory behavior of the classical MFS solution, due to the Gibbs phenomenon, is shown to vanish.



## 1. Introduction

The method of fundamental solutions (MFS) is a Trefftz type meshfree numerical method which can be applied for the approximate solution of certain boundary value problems (BVPs), usually with continuous boundary data, e.g. [1–4]. For smooth domains, spectral convergence has been proven in [5–7], in the 2D (or complex) case, assuming that the boundary condition is an analytic (entire) function.

However, when the boundary of the domain has singularities, e.g. corners, cracks, etc., or when the boundary conditions are not sufficiently regular, the analytic MFS shape functions prove to be inappropriate for fitting a possibly singular solution. While accuracy problems due to geometric singularities have been successfully addressed, e.g. [8,9], the lack of convergence of the MFS in the case of BVPs with singular boundary conditions has been somehow neglected in the MFS literature.

Most commonly, the Motz benchmark problem [10] is considered when newly developed meshfree methods are tested against BVPs with singular boundary conditions, e.g. [11,12]. In the Motz problem an abrupt change in the type of boundary condition occurs, from Dirichlet to Neumann, leading to discontinuities of the partial derivatives of the exact solution on the boundary. However, the solution of the BVP is globally continuous in the closure of the domain and this problem may

* Corresponding author at: CEMAT–IST, University of Lisbon, Av. Rovisco Pais 1, 1049-001 Lisbon, Portugal.
*E-mail addresses:* carlos.alves@math.ist.utl.pt, carlos.alves@math.tecnico.ulisboa.pt (C.J.S. Alves), ssv@math.ist.utl.pt (S.S. Valtchev).

http://dx.doi.org/10.1016/j.amc.2017.09.018
0096-3003/

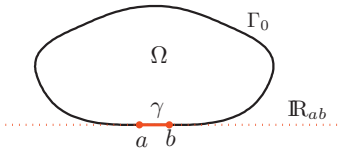


**Fig. 1.** Model problem settings in 2D.

be solved by adding particular solutions of the PDE, derived in polar coordinates, to the MFS approximation basis, as it has been done for the 2D Helmholtz BVP in [9].

In this work, we consider Dirichlet boundary conditions that may present a jump discontinuity in the function itself. Therefore, the exact solution of the BVP has a singular trace on the boundary which is a discontinuous function in the tangential direction. It is known that in this case the approximate solution by the MFS suffers from the Gibbs phenomenon, e.g. [13]. Also, in general, the type of singularity exhibited by the fundamental solution is different from the one shown by the exact solution and therefore no accurate numerical results may be achieved by the classical MFS, even if source points are taken arbitrarily close to the boundary. On the other hand, continuous particular solutions similar to the ones derived in [9] are also not appropriate for fitting the discontinuous Dirichlet boundary function.

In order to correctly recreate the discontinuity of the exact solution on the boundary we will include a set of exact solutions with discontinuous boundary traces in the MFS approximation basis. The definition of such special functions is motivated by the formulation of the classical boundary element method (BEM) and they can be derived analytically, by evaluating a double layer potential on a boundary segment.

This paper extends previous works by Alves and Leitão [8] and Antunes and Valtchev [9]. Here, the coupling with BEM is not in the sense of obtaining two different solutions by implementing two different methods (see for instance Tadeu et al. [14]), it is in the sense of adding a small number of BEM-type singularity-capturing basis functions to the MFS approximation space, while preserving all meshfree characteristics of the original method.

The technique presented here for the Laplace equation can be extended to other partial differential equations, with a known fundamental solution, provided the evaluation of the double layer potential on a boundary segment can be carried out analytically or numerically.

The paper is divided as follows. In Section 2 we briefly describe the subtraction of singularity approach and split the BVP into a regular and a discontinuous subproblem. In Section 3 we focus on the Dirichlet problem for the 2D Laplace equation, posed in a square domain and derive the special harmonic functions that will be used for the analytic solution of the singular subproblem. In Section 4, a modification of the classical MFS is presented, where the special harmonic functions derived in the previous section are appended to the approximation basis. Finally, in Section 5 we present numerical results that illustrate the performance of the two approaches.

## 2. Subtraction of singularity approach

Let $\Phi$ be a fundamental solution of the elliptic differential operator $\mathcal{L}$, with constant coefficients, thus satisfying, in the sense of distributions

$$\mathcal{L}\Phi = \delta,$$

where $\delta$ is the Dirac distribution.

It is well known, e.g. [1–3], that the method of fundamental solutions can be applied for the Dirichlet boundary value problem

$$(\mathcal{P})\begin{cases} \mathcal{L}u = 0 & \text{in } \Omega \\ u = \mathcal{G} & \text{on } \Gamma := \partial\Omega, \end{cases}$$

where $\Omega \subset \mathbb{R}^d$ $(d = 2, 3, \ldots)$ is a bounded simply connected domain, but its accuracy is greatly affected if the boundary data $\mathcal{G}$ is not represented by a sufficiently regular function. In particular, if the function $\mathcal{G}$ is discontinuous, the approximate solution presents a typical oscillatory behavior known as the Gibbs phenomenon, similar to the one observed for Fourier approximations of discontinuous functions, e.g. [13].

In this paper we will address only the 2D case, and therefore $\Gamma$ will be a closed curve, see Fig. 1. Also, in order to simplify the presentation, we will assume that $\mathcal{G}$ presents at most two discontinuities, located at the end points $a$ and $b$ of the straight line segment

$$\gamma := ]a, b[ = \{(1-t)a + t\,b : t \in ]0, 1[\} \subset \Gamma.$$

The function $\mathcal{G}$ can then be rewritten as:

$$\mathcal{G}(x) = \begin{cases} G(x) & \text{on } \Gamma_0 = \Gamma \backslash \bar{\gamma} \\ g(x) & \text{on } \gamma, \end{cases}$$

where $G$ and $g$ are regular functions, for example $G \in C^m(\Gamma_0)$ and $g \in C^m(\gamma)$, and at least one of the following conditions is true: $G(a) \neq g(a)$ or $G(b) \neq g(b)$.

**Remark 1.** For more complex domains we may consider that the straight line $\mathbb{R}_{ab} \supset \gamma$, see Fig. 1, is tangent to $\Gamma$ at the discontinuity point $a$ and take $b$ to be sufficiently close to $a$, with no jump at $b$. This approach may be used to generalize the process we present next for any number of discontinuities and an arbitrary convex domain.

For the subtraction of singularity approach to problem $(\mathcal{P})$ we consider the following three steps:

(1) Define a Hermite interpolating polynomial $P$ which extends $G$ to $\gamma$ as a function $\tilde{G}$

$$\tilde{G} = \begin{cases} G & \text{on } \Gamma_0 \\ P & \text{on } \gamma, \end{cases} \tag{1}$$

such that $\tilde{G} \in C^m(\Gamma)$.

(2) Approximate $g - P$ on $\gamma$ by a linear combination of special functions $\Psi_k$ that are particular solutions of the differential equation for a crack problem on $\gamma$, see Remark 2.
These functions are given by

$$\Psi_k(x) = \int_\gamma p_k(y) \frac{\partial \Phi}{\partial n_y}(x-y) ds_y, \tag{2}$$

where $p_0, p_1, \ldots$ is an arbitrary basis for the polynomial functions defined on $\gamma$. Note that, for their inner trace, these functions satisfy $\Psi_k(x) = p_k(x)$ for $x \in \gamma$.

**Remark 2.** We have $\Psi_k(x) = 0$ on $\mathbb{R}_{ab} \setminus [a, b]$, because $n_y \perp (x - y)$ and since the fundamental solution is a radially symmetric function, i.e. $\Phi(x) = \phi(||x||)$,

$$\frac{\partial \phi}{\partial n_y}(||x-y||) = n_y \cdot \frac{x-y}{||x-y||} \phi'(||x-y||) = 0, \quad x \in \mathbb{R}_{ab} \setminus [a, b],\ y \in ]a, b[,$$

noting that for $x \in \mathbb{R}_{ab} \setminus [a, b]$ the integral in (2) is regular.

Assuming that we can approximate $g - P$ by a linear combination of such functions, which is exact if $g$ is a polynomial of degree $2m + 1$:

$$g(x) - P(x) = \sum_{k=0}^{2m+1} \alpha_k p_k(x)$$

then the function

$$u_D(x) = \sum_{k=0}^{2m+1} \alpha_k \Psi_k(x)$$

is a particular solution of the differential equation, satisfies the boundary condition $u_D = g - P$ on $\gamma$, and it is null on $\mathbb{R}_{ab} \setminus [a, b]$.

(3) Apply the classical MFS to the differential equation with the new boundary data

$$\mathcal{G}_R = \begin{cases} G - u_D & \text{on } \Gamma_0 \\ P & \text{on } \gamma, \end{cases} \tag{3}$$

which is at least $C^m(\Gamma)$, to obtain the solution $u_R$. Note that $G - u_D = G$ near the crack tips, because $u_D \equiv 0$ on $\mathbb{R}_{ab} \setminus [a, b]$, see Remark 2.

It is then clear that the solution $u$ of problem $(\mathcal{P})$ is given by $u = u_R + u_D$ where

$$(\mathcal{P}_R) \begin{cases} \mathcal{L} u_R = 0 & \text{in } \Omega \\ u_R = G - u_D & \text{on } \Gamma_0 \\ u_R = P & \text{on } \gamma \end{cases} \qquad (\mathcal{P}_D) \begin{cases} \mathcal{L} u_D = 0 & \text{in } \Omega \\ u_D = u_D & \text{on } \Gamma_0 \\ u_D = g - P & \text{on } \gamma \end{cases} \tag{4}$$

**Remark 3.** The first step consists in a simple Hermite interpolation on a linear segment. The second step allows for the explicit calculation of $u_D$ which can be exact if $g$ is a polynomial function. If $g$ is non-polynomial, or if it can only be approximated by high degree polynomials, then we should consider smaller intervals, where the approximation holds. Finally, in the third step, since $\mathcal{G}_R$ can be as regular as required, the MFS is expected to perform with very high precision, giving the regular solution $u_R$.

The calculation of the functions $\Psi_k$ is usually performed in the context of the boundary element method (BEM) and next we present the explicit equations for $k = 0, 1, 2, 3$.

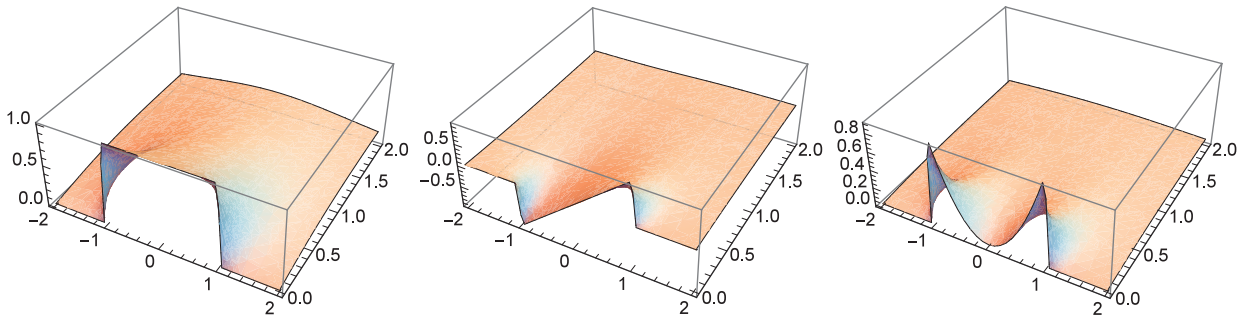

**Fig. 2.** The functions $\Psi_0$, $\Psi_1$ and $\Psi_2$, for $\gamma = ]-1, 1[\times\{0\}$.

### 2.1. Functions $\Psi_k$ for the Laplace equation

In the case of the Laplace equation, the fundamental solution is given by

$$\Phi(x) = -\frac{1}{2\pi}\log(||x||).$$

Considering a crack $\gamma = ]a, b[\times\{A\}$, the functions $\Psi_k$ can be derived in closed form by analytically evaluating the integral:

$$\Psi_k(x) = \int_a^b y_1^k \frac{\partial \Phi}{\partial n_y}(x-y)dy_1.$$

These functions satisfy, for their upper trace (which we assume here to be the inner trace)

$$\Psi_k(x_1, A) = \begin{cases} x_1^k & \text{if } x_1 \in ]a, b[ \quad \text{(i.e. if } (x_1, A) \in \gamma) \\ 0 & \text{if } x_1 \notin [a, b] \end{cases} \tag{5}$$

and in particular, for $k = 0, 1, 2, 3$, we have:

$$\Psi_0(x_1, x_2) = \frac{1}{\pi}\left(\arctan\frac{a-x_1}{A-x_2} - \arctan\frac{b-x_1}{A-x_2}\right), \tag{6}$$

$$\Psi_1(x) = x_1\Psi_0(x) + \frac{A-x_2}{2\pi}\log\left(\frac{(a-x_1)^2+(A-x_2)^2}{(b-x_1)^2+(A-x_2)^2}\right), \tag{7}$$

$$\Psi_2(x) = 2x_1\Psi_1(x) - ((A-x_2)^2+x_1^2)\Psi_0(x) + (A-x_2)\frac{a-b}{\pi}, \tag{8}$$

$$\Psi_3(x) = (3x_1^2-(A-x_2)^2)\Psi_1(x) - 2x_1(x_1^2+(A-x_2)^2)\Psi_0(x) + (A-x_2)\frac{a-b}{\pi}(a+b+4x_1). \tag{9}$$

Graphically, the first three functions, $\Psi_0, \Psi_1$ and $\Psi_2$, are represented in Fig. 2.

## 3. Laplace BVP in a square domain

To exemplify the procedure we consider the Laplace equation in $\Omega = (A, B)^2 \subset \mathbb{R}^2$ with a possibly discontinuous boundary condition on the boundary segment $\gamma = ]a, b[\times\{A\}$, and assuming that $[a, b] \subset ]A, B[$. In particular we consider

$$(\mathcal{P})\begin{cases} \Delta u = 0 & \text{in } \Omega \\ u = G & \text{on } \Gamma_0 \\ u = g & \text{on } \gamma \end{cases}$$

with $G$ and $g$ being at least continuous functions.

### 3.1. Continuous extension

The possible discontinuity points here are $(a, A)$ and $(b, A)$, and a simple linear interpolation provides a continuous extension of $G$ from $\Gamma_0$ to $\Gamma$ with

$$P(x_1, A) = G_a + \frac{G_b - G_a}{b-a}(x_1 - a), \quad \text{with } (x_1, A) \in \gamma, \tag{10}$$

where $G_a = G(a, A)$ and $G_b = G(b, A)$.

In the particular case when $g(x) = g_0 + g_1 x_1$ (with constants $g_0$ and $g_1$), the full solution of problem $(\mathcal{P}_D)$ can be obtained by replacing, in $g - P$, the constant function 1 by $\Psi_0(x)$ and $x_1$ by $\Psi_1(x)$, thus leading to

$$u_D(x) = (g_0 - G_a)\Psi_0(x) + g_1\Psi_1(x) - \frac{G_b - G_a}{b-a}(\Psi_1(x) - a\Psi_0(x)). \tag{11}$$

Now $u_D$ can be used to solve problem $(\mathcal{P}_R)$ by the MFS. Since the boundary function $\mathcal{G}_R$ is at least continuous, the approximate solution of problem $(\mathcal{P}_R)$ will have good accuracy and, in particular, no Gibbs effect perturbations will be present.

### 3.2. Higher regularity extension

The previous analysis can be extended to achieve higher regularity of $\mathcal{G}_R$. Using Newton's formula and defining $G_A(x) = G(x, A)$, the Hermite interpolation polynomial

$$P(x_1, A) = G_A(a) + G_A[a, a](x_1 - a) + G_A[a, a, b](x_1 - a)^2 + G_A[a, a, b, b](x_1 - a)^2(x_1 - b)$$

with $(x_1, A) \in \gamma$, guarantees that $\mathcal{G}_R \in C^1(\Gamma)$.

In particular, if $g$ is a third degree polynomial, then we can write

$$g(x_1, A) - P(x_1, A) = \beta_0 + \beta_1 x_1 + \beta_2 x_1^2 + \beta_3 x_1^3,$$

with $\beta_i \in \mathbb{R}$ and the solution $u_D$ of problem $(\mathcal{P}_D)$ is then explicitly given by

$$u_D = \beta_0\Psi_0 + \beta_1\Psi_1 + \beta_2\Psi_2 + \beta_3\Psi_3. \tag{12}$$

This improves to $C^1$ the regularity of $\mathcal{G}_R$ and the MFS approximate solution of problem $(\mathcal{P}_R)$ will exhibit even better accuracy than in the previous case.

**Remark 4.** Further improvement of the numerical results may be achieved by considering a higher regularity extension of $G$ on $\gamma$ but this approach requires the calculation of additional $\Psi_k$ functions which increases the computational cost of the method. Also, in the case when $g$ is not a third degree polynomial or a third degree polynomial approximation of $g$ is not sufficiently accurate, the method may be applied with $\gamma$ divided into a set of shorter segments.

## 4. Enriching the MFS basis

In the classical MFS we seek for an approximate solution $\tilde{u}$ of problem $(\mathcal{P})$ in the form of a linear combination

$$\tilde{u}(x) = \sum_{j=0}^{m} \alpha_j \phi_j(x), \quad x \in \bar{\Omega},$$

with coefficients $\mathbf{a} = (\alpha_0, \ldots, \alpha_m)$, where

$$\phi_j(x) = \begin{cases} 1 & j = 0 \\ \Phi(x - y_j) & j = 1, \ldots, m \end{cases}$$

and the singularities $\mathcal{Y} = \{y_1, \ldots, y_m\} \subset \hat{\Gamma}$ are taken on the boundary $\hat{\Gamma}$ of an admissible region $\hat{\Omega} \supset \bar{\Omega}$. Here, the constant function $\phi_0(x) = 1$ is included in the approximation space only for the sake of completeness, in the case of the Dirichlet problem for the 2D Laplace PDE, e.g. [15,16].

As described above, the classical MFS performs poorly and leads to inaccurate numerical results for the solution of problem $(\mathcal{P})$ since the analytic function $\tilde{u}$ cannot recreate correctly the discontinuity of the boundary condition.

It is possible to use the subtraction of singularity approach, presented in the previous sections, to overcome the discontinuity problem by splitting problem $(\mathcal{P})$ into a regular part $(\mathcal{P}_R)$, solved by the classical MFS, and a singular part $(\mathcal{P}_D)$, with solution expressed in terms of the basis $\{\Psi_0, \ldots, \Psi_p\}$. However, when $g$ is not a polynomial function, since $\Psi_k$ are polynomials on $\gamma$, problem $(\mathcal{P}_D)$ can only be solved approximately, for instance using collocation methods. Here, we want to avoid this extra computational effort, using an enrichment approach.

Thus, in this section we present a more compact, one step approach, that can be used to solve both problems $(\mathcal{P}_R)$ and $(\mathcal{P}_D)$ simultaneously. In particular, this approach will allow us to solve BVPs with a non-polynomial boundary condition $g$.

More precisely, we enrich the MFS approximation basis with a set of $p+1$ particular solutions $\Psi_0, \ldots, \Psi_p$, and consider the new basis:

$$\{\phi_0, \ldots, \phi_m\} \cup \{\Psi_0, \ldots, \Psi_p\},$$

for which the total solution $u$ of problem $(\mathcal{P})$ is approximated by

$$\tilde{u}(x) = \alpha_0 + \sum_{j=1}^{m} \alpha_j \phi_j(x) + \sum_{k=0}^{p} \beta_k \Psi_k(x), \quad x \in \bar{\Omega}. \tag{13}$$

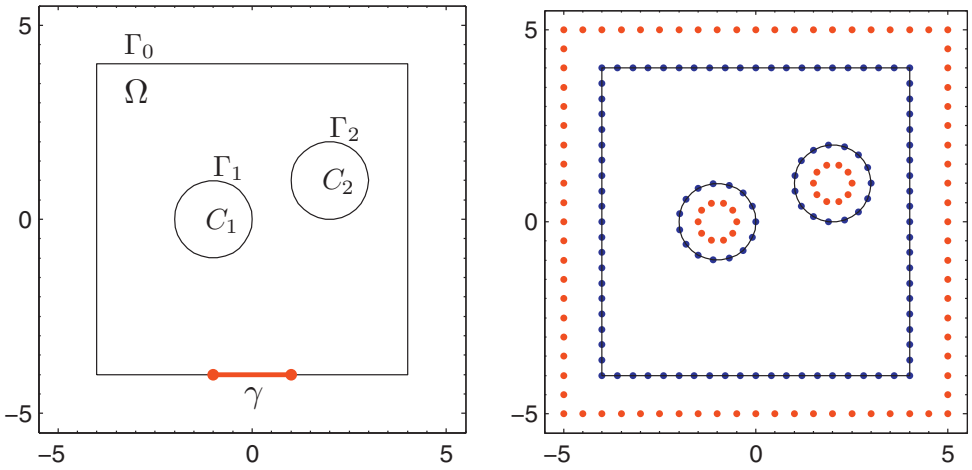


**Fig. 3.** The domain $\Omega$ for the test problem (left) and a sample distribution of collocation (blue dots) and source (red dots) points (right). (For interpretation of the references to color in this figure legend, the reader is referred to the web version of this article.)

The unknown coefficients $\mathbf{a}$ and $\mathbf{b} = (\beta_0, \ldots, \beta_p)$, are then determined by collocating (interpolating or fitting in the least squares sense) the boundary condition $\mathcal{G}$ over a set of $n$ boundary collocation points $\mathcal{X} = \{x_1, \ldots, x_n\} \subset \Gamma$ :

$$\begin{bmatrix} \phi_0(x_1) & \cdots & \phi_m(x_1) & \Psi_0(x_1) & \cdots & \Psi_p(x_1) \\ \vdots & \ddots & \vdots & \vdots & \ddots & \vdots \\ \phi_0(x_n) & \cdots & \phi_m(x_n) & \Psi_0(x_n) & \cdots & \Psi_p(x_n) \end{bmatrix} \begin{bmatrix} \mathbf{a} \\ \mathbf{b} \end{bmatrix} = \begin{bmatrix} \mathcal{G}(x_1) \\ \vdots \\ \mathcal{G}(x_n) \end{bmatrix}. \tag{14}$$

**Remark 5.** Numerical tests indicate that the coefficients $\mathbf{b}$ calculated trough the enriched MFS correspond to the coefficients of $u_D$ in (12), if $g$ is a polynomial function of degree $\leq p$. On the other hand, for a non-polynomial function $g$, the enriched MFS gives the best approximation of the solution of problem $(\mathcal{P})$ by collocation, where both $\phi_j$ and $\Psi_k$ functions contribute for the fitting of $\mathcal{G}$ on the total boundary $\Gamma$.

## 5. Numerical simulations

In order to illustrate and compare the performance of the numerical methods introduced in Sections 3 and 4, we will consider the following test problem

$$\begin{cases} \Delta u = 0 & \text{in } \Omega \\ u = G & \text{on } \Gamma \backslash \tilde{\gamma} \\ u = g & \text{on } \gamma \end{cases} \tag{15}$$

where $\Omega = [-4, 4]^2 \backslash (C_1 \cup C_2)$ is a square multiply-connected domain and the cut-outs $C_1$ and $C_2$ are two unitary discs, centered at $(-1, 0)$ and $(2, 1)$, respectively, see Fig. 3, left. Let $\Gamma = \partial\Omega$, $\Gamma_1 = \partial C_1$, $\Gamma_2 = \partial C_2$, $\gamma = [-1, 1] \times \{-4\}$ and denote by $\Gamma_0$ the remaining part of the boundary of the square. For this particular problem we set $A = -4$, $a = -1$ and $b = 1$ in the definition of $\Psi_k$, $k = 0, 1, 2, \ldots$, see Section 2.1.

A sample distribution for the collocation and source points is shown in Fig. 3, right. In particular, equally spaced knots will be considered in the numerical examples. For the pseudo boundary we took $\hat{\Gamma} = \partial\hat{\Omega}$, where $\hat{\Omega} \supset \Omega$ is a larger square $[-4 - \hat{d}, 4 + \hat{d}]^2 \supset [-4, 4]^2$ with two circular cut-outs, concentric with $C_1$ and $C_2$, and with radii $\hat{r} < 1$. Here, the values of $\hat{d} > 0$ and $0 < \hat{r} < 1$ may be varied in order to tune the accuracy of the method.

Since, for an arbitrary choice of the boundary functions $G$ and $g$, the exact solution $u$ of problem (15) is not available, the quality of the approximate solution $\tilde{u}$ will be evaluated in terms of the boundary error $\|u - \tilde{u}\|_{2,\Gamma}$. Here, the discrete $l^2$ norm, equivalent to the RMS error

$$\varepsilon_{2,\Gamma} := \|u - \tilde{u}\|_{2,\Gamma} = \left[ \frac{1}{\#\mathcal{Z}} \sum_{z \in \mathcal{Z}} |u(z) - \tilde{u}(z)|^2 \right]^{1/2},$$

with $\mathcal{Z} \subset \Gamma$ representing a set of error test points, will be used.

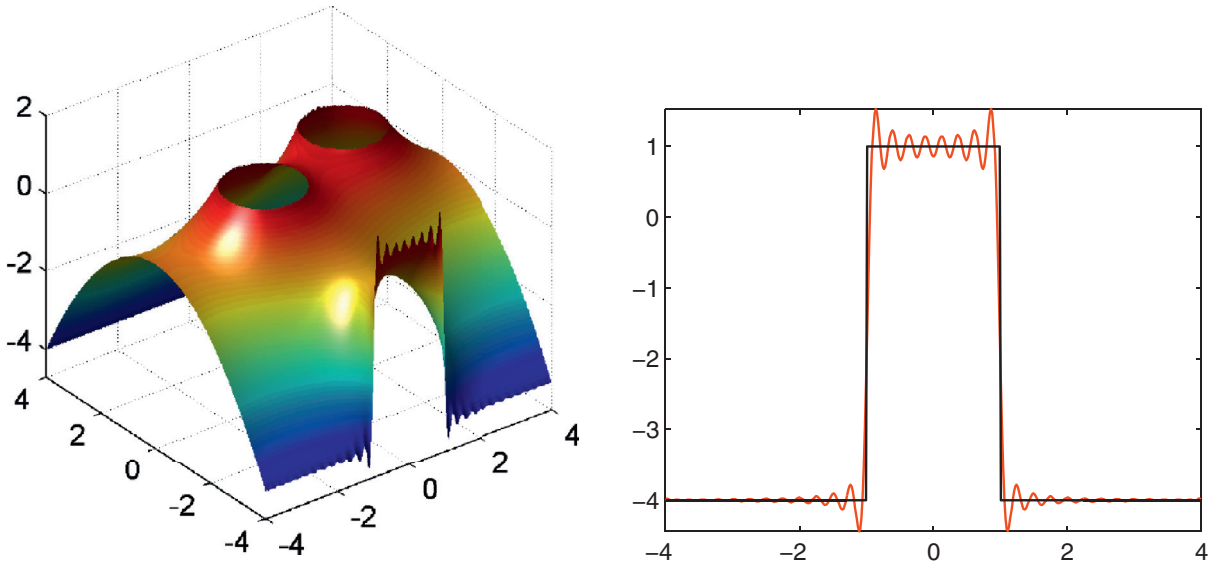


**Fig. 4.** Classical MFS: approximate solution in $\Omega$ (left) and exact (black) and approximate (red) solution on $[-4,4]\times\{-4\}$ (right). (For interpretation of the references to color in this figure legend, the reader is referred to the web version of this article.)

Before applying the numerical methods introduced in the previous sections we first illustrate the performance of the classical MFS for the test problem (15) with

$$G(x)=\begin{cases}-\frac{1}{4}x_2^2 & \text{on } \Gamma_0\\ 1 & \text{on } \Gamma_1\cup\Gamma_2\end{cases}\quad\text{and}\quad g(x)=1. \tag{16}$$

For $n=800$, $m=440$, $\hat{d}=1$ and $\hat{r}=0.5$ the resulting linear system was rank deficient ($rank=399$), due to the ill conditioning of the collocation linear system. Its residual error was 3.171, measured on the 2-norm, which led to a large boundary error of $\varepsilon_{2,\Gamma}=0.134371$. A plot of the approximate solution in $\Omega$ is shown in Fig. 4, left and an inappropriate oscillatory behavior can be observed near the jump discontinuities of the boundary condition. The occurrence of the Gibbs phenomenon is even more clear when we compare the exact and approximate solutions on the segment $[-4,4]\times\{-4\}$ of $\Gamma$, see Fig. 4, right.

### 5.1. Example 1 – constant function g(x)

Problem (15) with boundary conditions given by (16) will be considered here. The approaches described in Sections 3 and 4 will be applied and the numerical results will be compared with the approximate solution calculated by the finite element method (FEM).

#### 5.1.1. Subtraction of singularity approach

Since $G(-1,-4)=G(1,-4)=-4$, for this example, we can take $P(x)=-4$. In fact, this is the analytic continuation of $G$ on $\gamma$. Problem (15) may then be split into a regular and a discontinuous parts as described in Section 2:

$$(\mathcal{P}_R)\begin{cases}\Delta u_R=0 & \text{in } \Omega\\ u_R=G-u_D & \text{on } \Gamma\backslash\bar{\gamma}\\ u_R=-4 & \text{on } \gamma\end{cases}\quad(\mathcal{P}_D)\begin{cases}\Delta u_D=0 & \text{in } \Omega\\ u_D=u_D & \text{on } \Gamma\backslash\bar{\gamma}\\ u_D=5 & \text{on } \gamma\end{cases}. \tag{17}$$

The exact solution of problem $(\mathcal{P}_D)$ is then given by $u_D(x)=5\Psi_0(x)$ and in order to find the total solution $u=u_R+u_D$ it is sufficient to solve problem $(\mathcal{P}_R)$. The classical MFS will be used for this purpose.

For the previous knot configuration, i.e. $n=800$, $m=440$, $\hat{d}=1$ and $\hat{r}=0.5$, the MFS linear system corresponding to problem $(\mathcal{P}_R)$ was again rank-deficient ($rank=399$), but it was solved with a residual error of $1.77643\times10^{-5}$ which led to a boundary error of $\varepsilon_{2,\Gamma}=1.60439\times10^{-6}$. Since problem $(\mathcal{P}_D)$ was solved analytically, this value of $\varepsilon_{2,\Gamma}$ corresponds to the boundary error of the total solution. In other words, an improvement of approximately 5 orders of magnitude has been achieved, in comparison with the classical MFS solution. Note that the approximation error in the interior of the domain is even lower because the maximum principle holds for $u$ and $\tilde{u}$ and therefore for the absolute error function $|u-\tilde{u}|$.

A plot of the approximate solution $\tilde{u}=\tilde{u}_R+5\Psi_0$ in $\Omega$ is shown in Fig. 5, left.

In Fig. 5, right, we present a (semi-log scale) plot of the absolute error on the boundary of the square as a function of its arc-length $t\in[0,32[$. The absolute error on $\Gamma_1\cup\Gamma_2$ was approximately 3 orders of magnitude lower. It can be observed

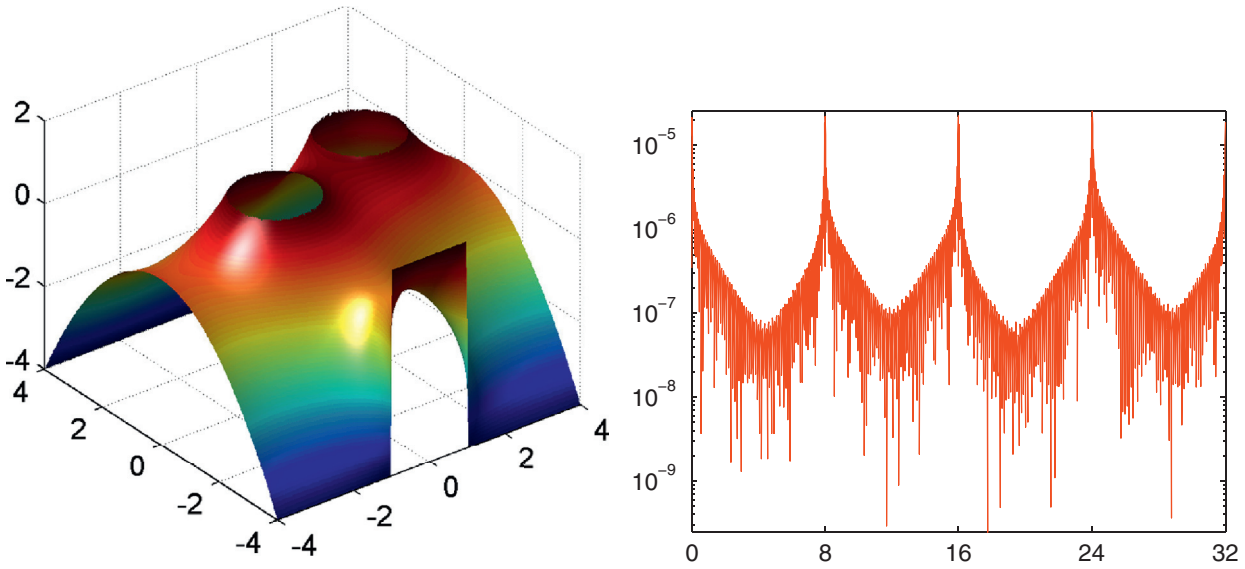


**Fig. 5.** The approximate solution $\tilde{u}$ in $\Omega$ (left) and the absolute error on the boundary of the square $[-4,4]^2$, as a function of its arc-length $t \in [0, 32[$ (right, semi-log scale).

that the maxima of the error now occur in the neighborhood of the corners of the domain ($t \in \{0, 8, 16, 24\}$) and no error peeks are present near the discontinuity points of the boundary condition ($t = 3$ and $t = 5$). Note that the accuracy problem near the corner points can be solved by adding appropriate singular shape functions, derived in polar coordinates, to the MFS approximation basis, see [9], but this is outside the scope of our paper.

*5.1.2. The enriched MFS*

The same BVP was also solved by the enriched MFS described in Section 4. In particular, the MFS approximation basis was augmented by the function $\Psi_0$.

For the same knot configuration as in the previous example the $800 \times 441$ linear system was rank-deficient ($rank = 400$), and it was solved with a residual error of $1.77484 \times 10^{-5}$ which led to a boundary error of $\varepsilon_{2,\Gamma} = 1.59933 \times 10^{-6}$. These numerical results are nearly identical to the ones presented in Section 5.1.1 which indicates that the two approaches are equivalent. In fact, the 2-norm distance between the two approximations, measured on $578,772$ uniformly distributed test points in $\bar{\Omega}$, was $8.16318 \times 10^{-8}$, which is two orders of magnitude lower than the corresponding RMS error of each approximation. Furthermore, the coefficient of $\Psi_0$ in the linear combination (13) was 5.0000000375 which deviates by $3.75 \times 10^{-8}$ from the expected value of 5, corresponding to the magnitude of the jump in the boundary condition at the points $(-1,-4)$ and $(1,-4)$.

We also analyzed the convergence of the enriched MFS with respect to the number of collocation and source points. Since the domain $\Omega$ and the boundary conditions present singularities, higher accuracy can be achieved if more collocation than source points are considered, i.e. if the collocation linear system is solved in the least squares sense. For the initial knot configuration, we took $n_1 = 20$ collocation points on each edge of the square $[-4,4]^2$ and $n_2 = 15$ on each circle $\Gamma_1$ and $\Gamma_2$. For the source points we took $m_1 = 10$ and $m_2 = 8$, with analogous meaning. The convergence analysis was then performed by increasing $n = \mu(4n_1 + 2n_2) = 110\mu$ and $m = \mu(4m_1 + 2m_2) = 56\mu$ with $\mu = 1, 2, \ldots$, preserving in this way the approximate ratio of 2: 1 between the number of collocation and source points. Note that the parameters $n$ and $m$ are interdependent and therefore it is not possible to achieve high accuracy by fixing one of them and increasing the other.

In Fig. 6 we present the semi-log plot of the RMS error as a function of the parameter $\mu = 1, 2, \ldots, 50$, for three choices of the distance $\hat{d}$ between the collocation and source points. Here, a fixed value of $\hat{r} = 0.5$ was considered since the boundary error on $\Gamma_1 \cup \Gamma_2$ is negligible in comparison with the error on $\Gamma_0$.

The numerical results indicate that the accuracy of the method increases when more collocation and source knots are considered. Also, for a fixed value of $\hat{d}$, there is an optimal number of points beyond which the improvement is only marginal or none. For example, for $\hat{d} = 0.50$ and $\mu = 15$ ($n = 1650$ and $n = 840$) the RMS error was $\varepsilon_{2,\Gamma} = 3.33542 \times 10^{-7}$ and no significant further error decrease was possible.

Higher accuracy may also be achieved by moving the source points closer to the domain, i.e. by decreasing the value of $\hat{d}$, see Fig. 6. This fact is due to the presence of a geometric singularity in $\Omega$ which induces singularities in the solution $u$ at the four corners of the domain. In this situation, better results can only be achieved by moving the singularities (source points) of the fundamental solutions closer to the corner points of the domain. For example, for $\hat{d} = 0.05$ we observed a RMS error of $\varepsilon_{2,\Gamma} = 8.13017 \times 10^{-9}$. However, this approach has a limited benefit due to the different nature of the two types of singularities.

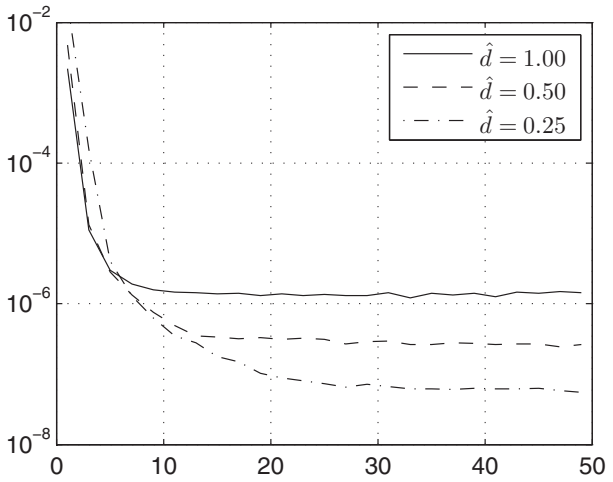


**Fig. 6.** The RMS boundary error as a function of $\mu = 1, \ldots, 50$, for several values of $\hat{d}$ (semi-log scale).

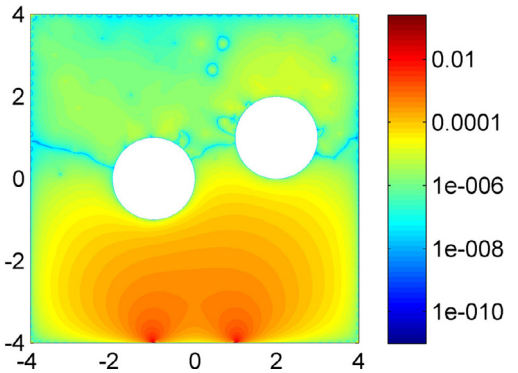


**Fig. 7.** The distance between the MFS and FEM approximate solutions (log scale).

**Table 1**
Convergence of the FEM approximation towards the MFS approximation.

| $N$ | DOF | $h$ | $\varepsilon_2$ | Rate |
|---|---|---|---|---|
| 0 | 40, 775 | 0.059555 | $2.22382 \times 10^{-3}$ | *** |
| 1 | 162, 191 | 0.029778 | $1.13932 \times 10^{-3}$ | 0.965 |
| 2 | 646, 943 | 0.014889 | $5.81407 \times 10^{-4}$ | 0.971 |
| 3 | 2, 584, 127 | 0.0077773 | $2.96026 \times 10^{-4}$ | 1.03 |

*5.1.3. Comparison with the FEM solution*

The same BVP was also implemented and solved using linear finite elements. In particular, for 646, 943 degrees of freedom (DOF), corresponding to a mesh of 1, 290, 240 triangles, the finite element method (FEM) produced an approximate solution $\tilde{u}^{FEM}$ that is visually identical to the solutions presented in Fig. 5, left. However, the distance between the FEM and the MFS solutions, measured on the RMS norm, was $\|\tilde{u} - \tilde{u}^{FEM}\|_{2,\bar{\Omega}} = 5.81407 \times 10^{-4}$. Noting that the MFS approximation from Section 5.1.1 has a domain error $\varepsilon_{2,\bar{\Omega}} \leq \varepsilon_{2,\Gamma} = 1.60439 \times 10^{-6}$, the calculated distance between the two approximate solutions may be viewed as the RMS error of the FEM solution.

As expected, the FEM struggles to approximate the solution of the BVP in the neighborhood of the endpoints of $\gamma$, which affects (locally) the accuracy. This fact is illustrated in Fig. 7, where we present a density plot of the distance $|\tilde{u} - \tilde{u}^{FEM}|$ between the two approximations in $\bar{\Omega}$.

Further numerical test indicate that the FEM approximation converges linearly (on the RMS norm) to the MFS solution, see Table 1. For this analysis, we considered an initial mesh ($N = 0$) of 40, 775 elements and the successive refinements ($N = 1, 2, 3$) were performed by sub-dividing each triangle into 4 new ones, using the midpoints of its edges.

Note that, by its definition, the FEM approximation is continuous in $\bar{\Omega}$ and therefore it does not converge, on the maximum norm, to the exact solution of the BVP. For all tested meshes, two peaks of the absolute error, with approximate magnitude of 0.25245, were observed at the boundary points $(-1, -4)$ and $(1, -4)$.

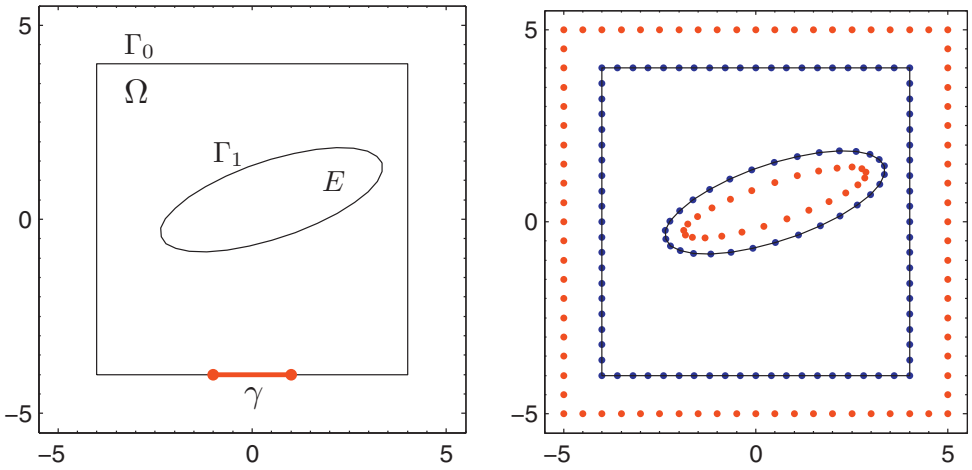


**Fig. 8.** The domain $\Omega$ (left) and a sample distribution of collocation and source points (right).

### 5.2. Example 2 – third order polynomial function g(x)

For this simulation we took the domain $\Omega = [-4,4]^2 \backslash E$, where $E$ is an ellipse with semi-axis $(a,b) = (3,1)$, center $c = (\frac{1}{2}, \frac{1}{2})$ and tilt angle $\alpha = \arctan(\frac{1}{3})$, defined by the following parameterization:

$$E = \{(x,y) = c + a\cos(t)u + b\sin(t)v : \ t \in [0, 2\pi]\},$$

with $u = (\cos(\alpha), \sin(\alpha))$ and $v = (-\sin(\alpha), \cos(\alpha))$, see Fig. 8, left. This particular choice for the ellipse $E$ was motivated by the relative position of the circles $C_1$ and $C_2$ in example 1. Here $c$ is the midpoint of the linear segment connecting the centers of the two circles and $\alpha$ is the segment's tilt angle.

The collocation and source points on the square boundaries were selected as before. The source points in $E$ were selected on a smaller ellipse with semi-axis (2.75, 0.75). The collocation and source points on the elliptic parts of $\Gamma$ and $\hat{\Gamma}$ were equally spaced with respect to the parameter $t$ in the corresponding parameterization, see Fig. 8, right.

We will consider a non-polynomial boundary function $G$ and a third order polynomial function $g$, given by:

$$G(x) = \begin{cases} \sin(\pi x_1) + \sin(\pi x_2) & \text{on } \Gamma_0 \\ -2 & \text{on } \Gamma_1 \end{cases} \quad \text{and} \quad g(x) = \sum_{i=0}^{3} a_i x_1^i, \tag{18}$$

where $a_i \in \mathbb{R}, \ i = 0,1,2,3$.

#### 5.2.1. Subtraction of singularity approach – continuous extension of G on $\gamma$

Noting that $G(-1,-4) = G(1,-4) = 0$, we can take $P(x) = 0$ in order to obtain a continuous extension of $G$ on $\gamma$, see Fig. 9, left. Consequently, the exact solution of problem $(\mathcal{P}_D)$ is given by $u_D(x) = \sum_{i=1}^{3} a_i \Psi_i(x), \ x \in \bar{\Omega}$.

For the particular choice of $g(x) = 2(1 - x_1 + x_1^3)$, see Fig. 9, left, the exact solution of problem $(\mathcal{P}_D)$ in $\bar{\Omega}$ is $u_D = 2(\Psi_0 - \Psi_1 + \Psi_3)$ and it remains to solve problem $(\mathcal{P}_R)$ using the classical MFS.

As before, we kept the ratio of 2: 1 between the collocation and source points and took approximately 30 collocation points per unit length on $\Gamma$. In particular, for $n_1 = 225, \ n_2 = 375, \ m_1 = 120, \ m_2 = 195$ and $\hat{d} = 0.15$, the $1275 \times 676$ linear system was solved with a residual error of $2.2744 \times 10^{-2}$ which led to a RMS error of $\varepsilon_{2,\Gamma} = 8.34545 \times 10^{-4}$ on the boundary $\Gamma$.

The absolute error of the approximate solution was of order $10^{-8}$ everywhere on $\Gamma$ except on the edge $[-4,4] \times \{-4\}$ where its order was $10^{-2}$, see Fig. 9, right. Note that the boundary condition in problem $(\mathcal{P}_R)$ is only continuous and therefore the analytic fundamental solutions are once again not sufficient for its approximation, especially in the neighborhood of the gradient's singularities.

Finally, the total approximate solution may be calculated as $\tilde{u} = \tilde{u}_R + u_D$ and its error corresponds to the RMS error of $\tilde{u}_R$.

#### 5.2.2. Subtraction of singularity approach – $C^1$ extension of G on $\gamma$

Since $G(-1,-4) = G(1,-4) = 0$ and $\frac{\partial G}{\partial x_1}(-1,-4) = \frac{\partial G}{\partial x_1}(1,-4) = -\pi$, the Hermite polynomial that corresponds to the $C^1$ extension of $G$ on $\gamma$ is given by $P(x) = \frac{\pi}{2}(x_1 - x_1^3)$, see Fig. 10, left. Consequently, the exact solution of problem $(\mathcal{P}_D)$ is given by $u_D = 2\Psi_0 - (2 + \frac{\pi}{2})\Psi_1 + (2 + \frac{\pi}{2})\Psi_3, \ x \in \bar{\Omega}$.

The higher regularity of the boundary conditions of problem $(\mathcal{P}_R)$ led to a more accurate MFS solution. For the same knot configuration as in the previous simulation ($n_1 = 225, \ n_2 = 375, \ m_1 = 120, \ m_2 = 195$ and $\hat{d} = 0.15$) the resulting linear

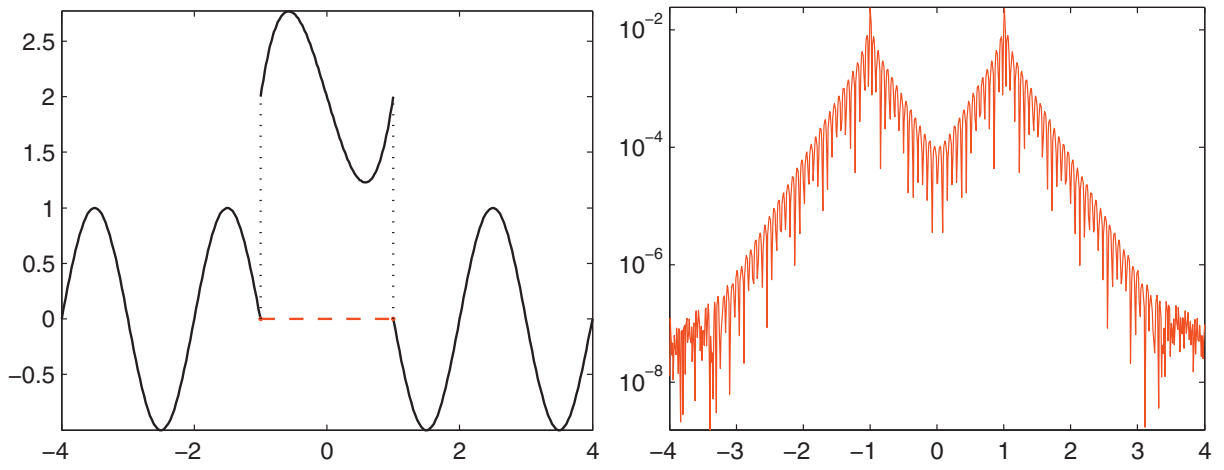

**Fig. 9.** Left plot: the boundary condition on $[-4,4]\times\{-4\}$ (solid line) and the continuous extension of $G$ on $\gamma$ (red, dashed line). Right plot: the absolute error of $\tilde{u}_R$ on $[-4,4]\times\{-4\}$. (For interpretation of the references to color in this figure legend, the reader is referred to the web version of this article.)

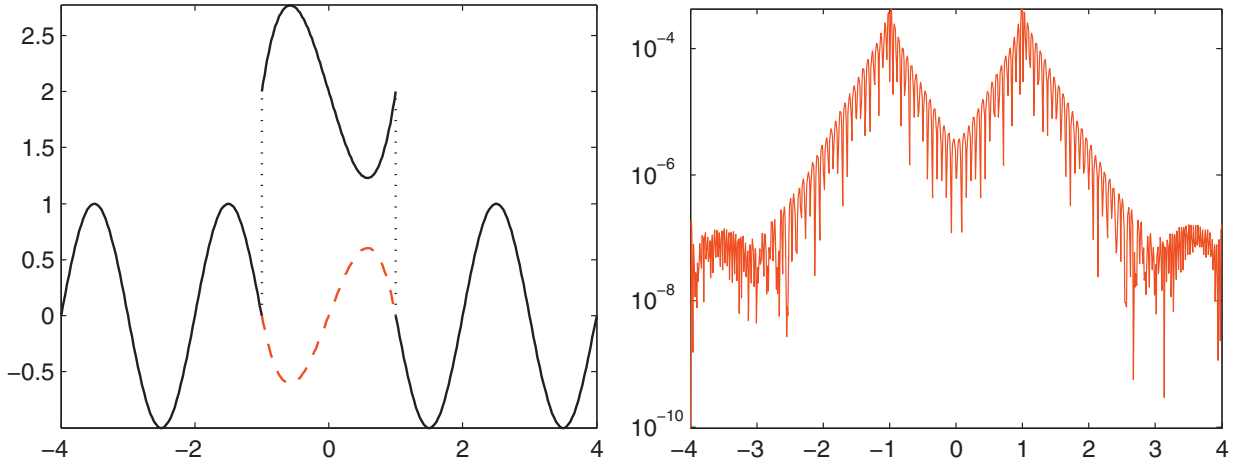

**Fig. 10.** Left plot: the boundary condition on $[-4,4]\times\{-4\}$ (solid line) and class $C^1$ extension of $G$ on $\gamma$ (red, dashed line). Right plot: the absolute error of $\tilde{u}_R$ on $[-4,4]\times\{-4\}$. (For interpretation of the references to color in this figure legend, the reader is referred to the web version of this article.)

system was solved with a residual error of $1.02601\times10^{-3}$ and the corresponding boundary RMS error was $\varepsilon_{2,\Gamma}=2.63953\times10^{-5}$. This value corresponds to a decrease by a factor of 32, in comparison with the previous result.

A decrease of the absolute error on $\Gamma$ was also observed. As expected, its maxima occurred on the segment $[-4,4]\times\{-4\}$, but in this simulation they were of order $10^{-4}$, that is 2 orders of magnitude lower than the previous result, see Fig. 10, right. The absolute error of $\tilde{u}_R$ on the rest of the boundary was more than 3 orders of magnitude lower.

Better numerical results can be achieved by increasing the number of collocation and source points, indicating that the method converges with respect to these parameters. For example, for $n_1=1125$, $n_2=1875$, $m_1=600$, $m_2=975$ and $\hat{d}=0.15$, the boundary RMS error of $\tilde{u}_R$ was $\varepsilon_{2,\Gamma}=2.0024\times10^{-6}$. However, a relatively larger, $6375\times3376$, linear system had to be solved in this simulation.

In alternative, a higher order Hermite polynomial may be considered in order to achieve a more regular extension of $G$ on $\gamma$. For example, $P(x)=\frac{7\pi}{8}x-\frac{5\pi}{4}x^3+\frac{3\pi}{8}x^5$ provides a class $C^2$ extension of the boundary condition. In this case, for $n_1=525$, $n_2=875$, $m_1=280$, $m_2=455$ and $\hat{d}=0.15$, the boundary RMS error of $\tilde{u}_R$ was $\varepsilon_{2,\Gamma}=5.88791\times10^{-8}$ and its maximum absolute error was $1.35015\times10^{-6}$. These values correspond to an improvement of more than two orders of magnitude in comparison with the previous results, while the dimensions of the linear system were only $2975\times1576$.

**Remark 6.** In the limiting case, we may consider the natural (analytic) extension of $G$ on $\gamma$, i.e. $P=G$, hoping to recover the optimal accuracy of the classical MFS. However, in this scenario, the exact solution of problem $(\mathcal{P}_D)$ can be calculated only if $G$ is a polynomial function on $\gamma$, which is a rather strong restriction.

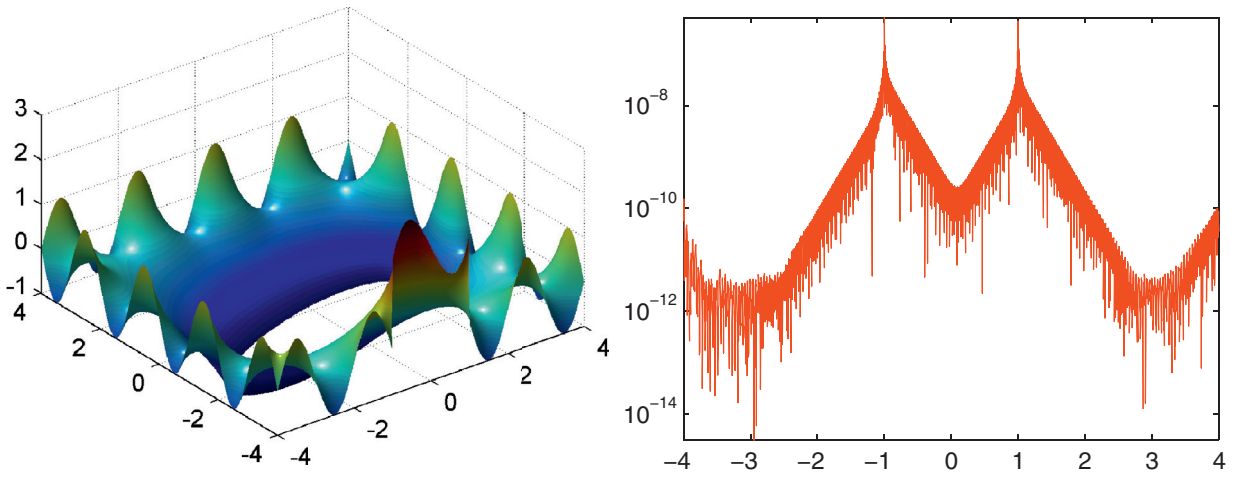


**Fig. 11.** The approximate solution $\tilde{u}$ in $\bar{\Omega}$ (left) and the absolute error on $[-4,4]\times\{-4\}$ (right).

*5.2.3. The enriched MFS*

Here, the MFS approximation basis was augmented by the function $\Psi_0,\ldots,\Psi_3$, in accordance with the degree of the polynomial boundary function $g$.

For the same knot configuration as in Section 5.2.2, i.e. $n_1=225$, $n_2=375$, $m_1=120$, $m_2=195$ and $\hat{d}=0.15$, the corresponding $1275\times 680$ linear system was solved with a residual error of $2.55346\times 10^{-4}$, which led to a boundary RMS error of $\varepsilon_{2,\Gamma}=2.06531\times 10^{-5}$. These numerical results are slightly better than the ones obtained in Section 5.2.2. This fact is due to the contribution of the extra basis functions for the global approximation of the solution.

Besides the usual convergence of the enriched MFS with respect to the number of collocation and source points, the accuracy of the results may also be improved by adding higher order $\Psi_i$ functions to the basis. For example, keeping the knot configuration from the previous simulation, we added the two functions $\Psi_4$ and $\Psi_5$ to the basis. The corresponding $1275\times 682$ linear system was solved with a residual error of $7.6854\times 10^{-6}$ which let to a RMS boundary error of $\varepsilon_{2,\Gamma}=8.09626\times 10^{-7}$. These values correspond to a decrease of nearly 2 orders of magnitude of the RMS error, while the computational cost of the method remained approximately the same. Note that adding two extra basis functions corresponds to adding two extra columns to the collocation matrix.

Further improvement of the numerical results may be achieved by combining an increase of the number of extra shape functions with an increase of the number of collocation and source points. For example, for $n_1=825$, $n_2=1375$, $m_1=440$, $m_2=715$ and 6 shape functions $\Psi_0,\ldots,\Psi_5$ we calculated the approximate solution with a boundary RMS error of $\varepsilon_{2,\Gamma}=8.54327\times 10^{-9}$ and a maximum absolute error of $5.18489\times 10^{-7}$, see Fig. 11, right. The approximate solution in $\bar{\Omega}$ is shown on Fig. 11, left.

*5.3. Example 3 – non-polynomial function g(x)*

For the last simulation we considered the same domain $\Omega=[-4,4]^2\backslash E$ as in the previous example but we took the following Dirichlet boundary condition:

$$G(x)=\begin{cases}\sin(\pi x_1)+\sin(\pi x_2) & \text{on } \Gamma_0\\ -2 & \text{on } \Gamma_1\end{cases}\quad\text{and}\quad g(x)=x_1+\frac{\sqrt{2-x_1}}{5}\sin(4\pi x_1), \tag{19}$$

where $g$ is a non-polynomial function, see Fig. 12, left. Note that, in this case, $g-P$ is not a polynomial function and problem $(\mathcal{P}_D)$ can not be solved analytically.

The enriched MFS, on the other hand, addresses the regular and discontinuous problems simultaneously. The extra shape functions $\Psi_k,\ k=0,\ldots,p$, absorb the singular behavior of the solution in the neighborhood of the jump discontinuities while the fundamental solutions $\phi_j,\ j=0,\ldots,m$, interpolate its smooth reminder. This combination of the two types of approximation allows us to solve accurately BVPs where $g$ is a non-polynomial function by adding relatively few $\Psi_k$ functions to the MFS basis.

For $n_1=150$, $n_2=250$, $m_1=80$, $m_2=130$ and $p=3$ we measured a RMS error of $\varepsilon_{2,\Gamma}=5.14141\times 10^{-4}$ which is already a satisfactory result since the domain error is even lower because of the maximum principle. Further improvement of the accuracy of the enriched MFS may be achieved by increasing the number of collocation and source points and by adding more $\Psi_k$ functions to the basis. For example, for $n_1=750$, $n_2=1250$, $m_1=400$, $m_2=650$ and $p=5$, the RMS error decreased by approximately 3 orders of magnitude to $\varepsilon_{2,\Gamma}=6.81862\times 10^{-7}$. The corresponding plot of the absolute error on the boundary segment $[-4,4]\times\{-4\}$ is shown in Fig. 12, right.

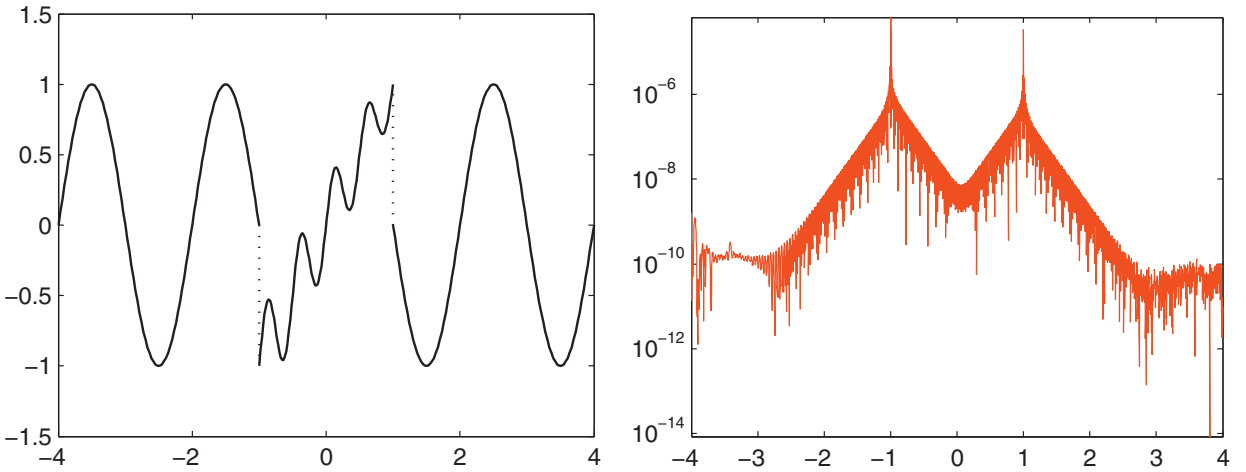


**Fig. 12.** The boundary condition on $[-4,4]\times\{-4\}$ (left) and the absolute error of $\tilde{u}$ on $[-4,4]\times\{-4\}$ (right).

## 6. Conclusions

Two numerical schemes, based upon the classical MFS, have been presented for the approximate solution of Laplace BVPs with discontinuous Dirichlet type boundary conditions. In the first case a subtraction of singularity approach was used. In the second, the approximation basis of the MFS was enriched with a set of harmonic functions with discontinuous traces on the domain's boundary.

The numerical results by both methods show significant improvement in comparison to the results with the classical MFS. In particular, no Gibbs type perturbation of the approximate solutions were observed.

An advantage of the enriched MFS method is that its application does not require the explicit calculation of the extension $P$ of the boundary condition $G$ on $\gamma$, as needed in the subtraction of singularity approach. In the enriched MFS method, the total solution of the BVP is calculated and both types of basis functions ($\phi_j$ and $\Psi_k$) contribute simultaneously to the approximation of its regular and singular behavior.

In general, if $g$ is a polynomial of order $p$, in the two step method we need $\Psi_k$ with $k=0,\ldots,p$ in order to solve problem $(\mathcal{P}_D)$ exactly. In this case, the accuracy of the two step method will be similar to the one of the enriched MFS with the same set of extra basis functions. On the other hand, the results by the enriched MFS can be improved significantly by adding higher order $\Psi_k$ functions to its basis. This approach requires much lower computational effort than increasing the number of collocation and source points.

## Acknowledgments

The financial support received from the Fundação para a Ciencia e a Tecnologia (FCT) project UID/Multi/04621/2013 is gratefully acknowledged.

## References

[1] G. Fairweather, A. Karageorghis, The method of fundamental solutions for elliptic boundary value problems, Adv. Comput. Math. 9 (1998) 69–95.
[2] G. Fairweather, A. Karageorghis, P.A. Martin, The method of fundamental solutions for scattering and radiation problems, Eng. Anal. Bound. Elem. 27 (2003) 759–769.
[3] M.A. Golberg, C.S. Chen, The Method of Fundamental Solutions for Potential, Helmholtz and Diffusion Problems, WIT Press, Computational Mechanics Publications, pp. 103–176.
[4] A. Karageorghis, D. Lesnic, L. Marin, A survey of applications of the MFS to inverse problems, Inverse Probl. Sci. Eng. 19 (3) (2011) 309–336.
[5] M. Katsurada, H. Okamoto, A mathematical study for the charge simulation method I, J. Fac. Sci. Univ. Tokyo Sect. 1A Math. 35 (1988) 507–518.
[6] X. Li, On convergence of the method of fundamental solutions for solving the Dirichlet problem of Poisson's equation, Adv. Comput. Math. 23 (3) (2005) 265–277.
[7] A. Barnett, T. Betcke, Stability and convergence of the method of fundamental solutions for Helmholtz problems on analytic domains, J. Comput. Phys. 227 (14) (2008) 7003–7026.
[8] C.J.S. Alves, V.M.A. Leitão, Crack analysis using an enriched MFS domain decomposition technique, Eng. Anal. Bound. Elem. 30 (2006) 160–166.
[9] P.R.S. Antunes, S.S. Valtchev, A meshfree numerical method for acoustic wave propagation problems in planar domains with corners and cracks, J. Comput. Appl. Math. 234 (9) (2010) 2646–2662.
[10] H. Motz, The treatment of singularities of partial differential equations by relaxation methods, Q. Appl. Math. 4 (4) (1947) 371–377.
[11] A. Karageorghis, Modified methods of fundamental solutions for harmonic and biharmonic problems with boundary singularities, Numer. Methods Partial Differ. Equ. 8 (1992) 1–19.
[12] A. Poullikkas, A. Karageorghis, G. Georgiou, Methods of fundamental solutions for harmonic and bi-harmonic boundary value problems, Comput. Mech. 21 (1998) 416–423.
[13] J.-H. Jung, A note on the Gibbs phenomenon with multiquadric radial basis functions, Appl. Numer. Math. 57 (2) (2007) 213–229.

[14] A. Tadeu, N. Simões, I. Simões, Coupling BEM/TBEM and MFS for the simulation of transient conduction heat transfer, Int. J. Numer. Methods Eng. 84 (2) (2010) 179–213.
[15] C.J. Alves, On the choice of source points in the method of fundamental solutions, Eng. Anal. Bound. Elem. 33 (12) (2009) 1348–1361.
[16] J.-T. Chen, J.-L. Yang, Y.-T. Lee, Y.-L. Chang, Formulation of the MFS for the two-dimensional laplace equation with an added constant and constraint, Eng. Anal. Bound. Elem. 46 (2014) 96–107.